Supporting Information for

The Single-Molecule Electrical Conductance of a Rotaxane-Hexayne Supramolecular Assembly

David C. Milan,[a,#] Maximilian Krempe,[b,#] Ali K. Ismael,[c,d,#] Levon D. Movsisyan,[e,#] Michael Franz,[b,#] Iain Grace,[c] Richard J. Brooke,[f] Walther Schwarzacher,[f]

Simon J. Higgins,[a,*] Harry L. Anderson,[e,*] Colin J. Lambert,[c,*] Rik R. Tykwinski,[b,*] Richard J. Nichols,[a,*]

[a] Department of Chemistry, University of Liverpool, Crown St, Liverpool, L69 7ZD, United Kingdom

[b] Department of Chemistry and Pharmacy & Interdisciplinary Center for Molecular Materials (ICMM), University of Erlangen-Nürnberg (FAU), Henkestrasse 42, 91054 Erlangen, Germany

[c] Department of Physics, University of Lancaster, Lancaster, LA1 4YB, U.K.

[d] Department of Physics, College of Education for Pure Science, Tikrit University, Tikrit, Iraq

[e] Department of Chemistry, University of Oxford, Chemistry Research Laboratory, Oxford, OX1 3TA, United Kingdom

[f] H. H. Wills Physics Laboratory, University of Bristol, Tyndall Avenue, Bristol BS8 1TL, United Kingdom

# These authors contributed equally to this work.

* Contact these author for correspondence

Table of Contents

1. Binding distance of Rotaxane and Dumbbell on a gold surface

To calculate the optimum binding distance for **3** and **3·M1** between two Au(111) surfaces we use DFT and the counterpoise method, which removes basis set superposition errors (BSSE). The binding distance d is defined as the distance between the gold surface and the nitrogen atom of the pyridyl group. Here molecule **3·M1** or **3** are defined as entity A and the gold electrodes as entity B.

The ground state energy of the total system is calculated using SIESTA and is denoted E_{AB}^{AB}, with the DFT parameters defined as those in the method section of the main text. Here the gold leads consist of 3 layers of 25 atoms. The energy of each entity is then calculated in a fixed basis, which is achieved through the use of ghost atoms in SIESTA. Hence the energy of the individual **3·M1** or **3** molecules in the presence of the fixed basis is defined as E_A^{AB} and for the gold as E_B^{AB}. The binding energy is then calculated using the following equation:

$$\text{Binding Energy} = E_{AB}^{AB} - E_A^{AB} - E_B^{AB} \qquad \text{(S1)}$$

Fig. **S1** shows that for the optimum binding distance d is 2.4 Å for both molecules and the binding energy is approximately 0.35 eV.

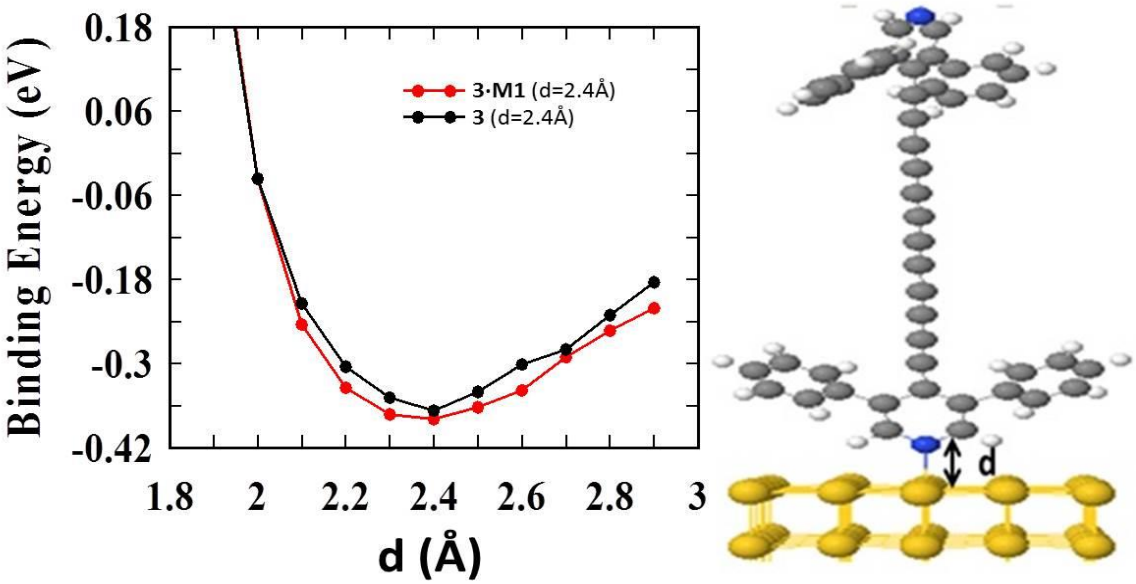

Figure S1. Binding energy of **3·M1** and **3** on a gold surface. Right panel: Orientation of **3** with respect to the gold leads.

2. Transmission coefficient as a function of macrocycle position and orientation along the dumbbell

We next investigate the effect of the position and orientation of the rotaxane ring along the axis. Fig. **S2** shows the effect of shifting the macrocycle along the length of **3**, starting from one end and progressively moving to the other, (i.e., from *z* = +3 Å to –3 Å along **3**, where *z* = 0 corresponds to half way along the oligoyne chain). The transmission curves show that there is a strong interaction between the 2,6-phenyl substituents of the pyridyl groups and the macrocycle only at *z* = ± 3 Å (i.e., where the transmission curves are significantly altered). This only changes the transmission close to the HOMO resonances, which is well away from the Fermi energy.

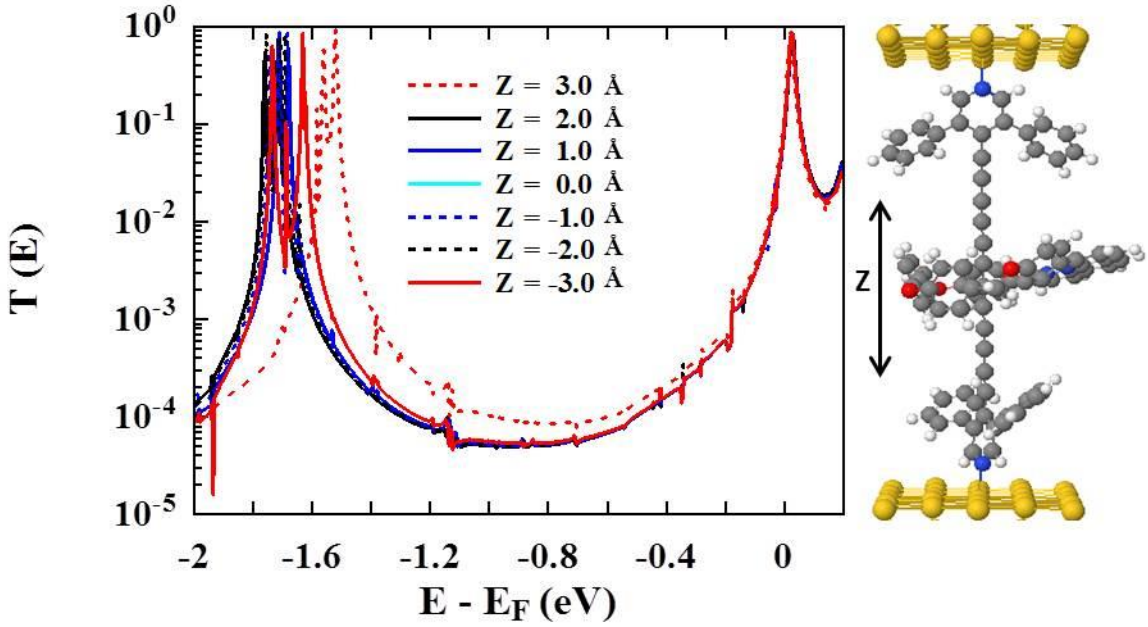

Figure S2. Transmission coefficient as a function of shifting the **3·M1** ring along the **3**. Transmission curves, $T(E)$, for seven different positions (ends when the ring is close to the anchor groups, 0 when the ring in the middle).

Figure **S3** shows the effect of shifting the orientation of the macrocycle around **3** for $\theta = 0°$ and 300° at *z* = 0, and it can be seen that there is no effect due to the rotation.

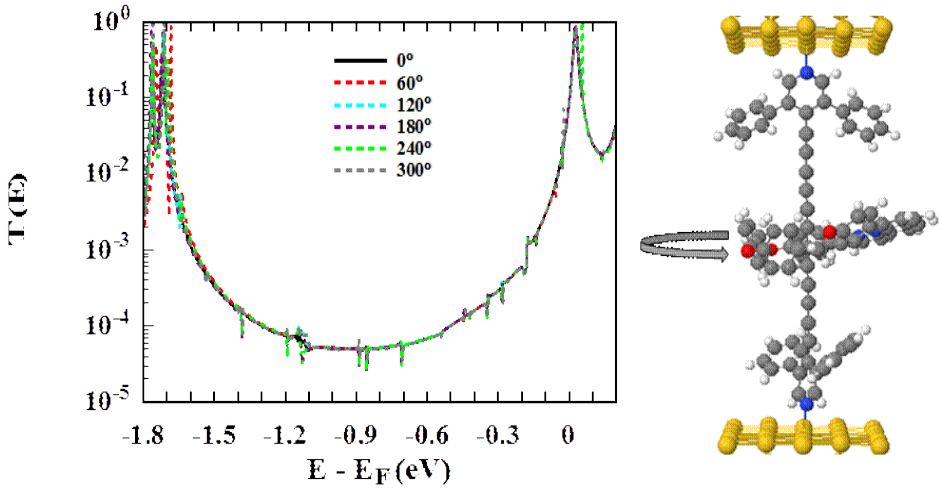

Figure S3. Transmission coefficient as a function of orientation. Zero bias transmission coefficient $T(E)$ versus electron energy E for rotation angles θ between 0° and 300° of the the rotaxane ring with respect to the **3**.

3. Frontier Orbitals

Plots of the frontier orbitals of **3** and **3·M1** are shown in Figures **S4** and **S5**. The results show that for **3·M1**, orbitals from HOMO to HOMO-4 inclusive are localised on the ring, while the HOMO-5 orbital has a similar energy to the HOMO of isolated **3** and is localised along the oligoyne backbone.

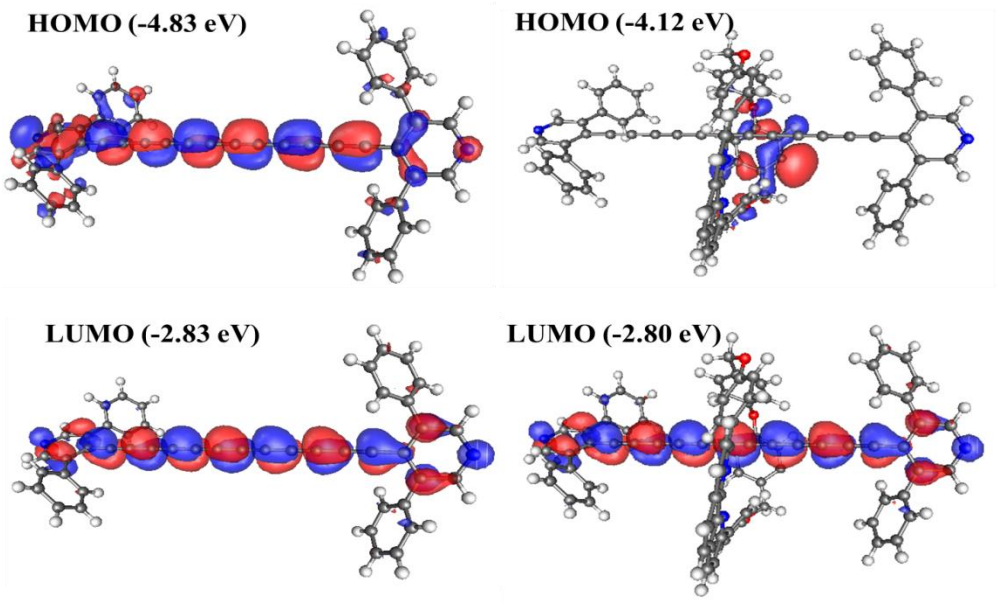

Figure S4. HOMO and LUMO orbitals of (left) **3** and (right) **3·M1**.

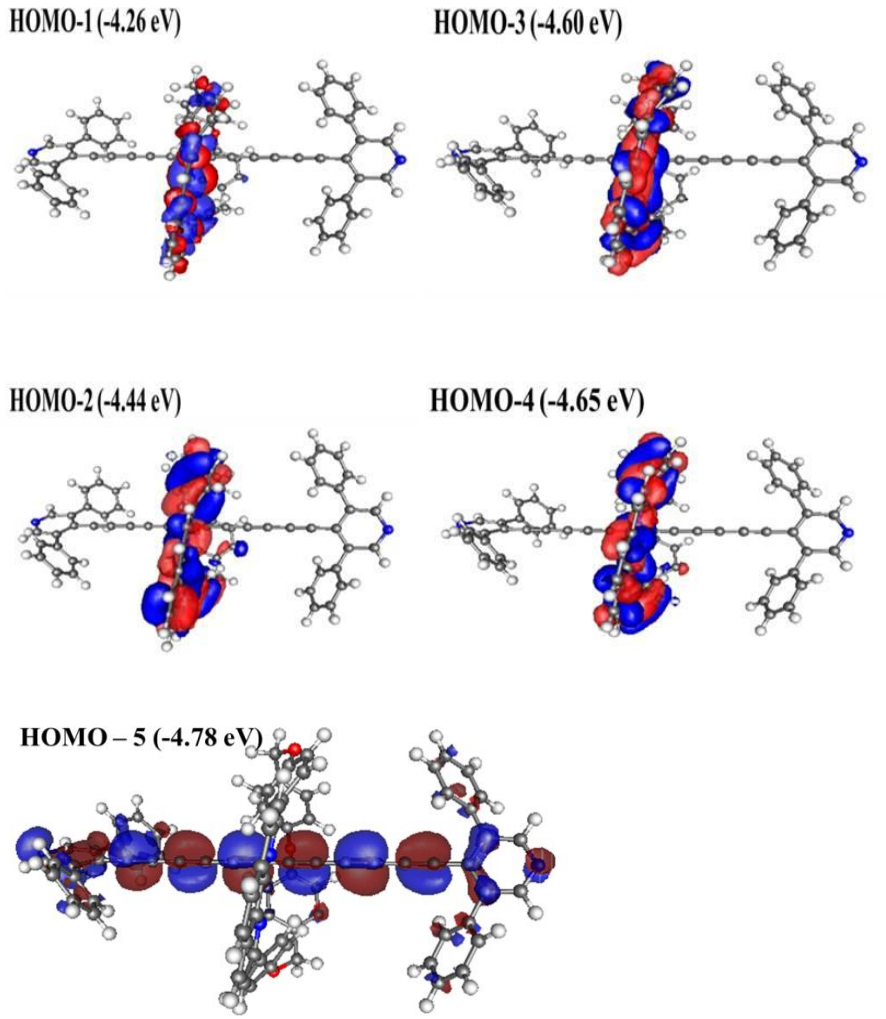

Figure S5. HOMO orbitals of the **3·M1**.

4. Synthesis and characterization

General procedures and methods:

Reagent grade chemicals were purchased from commercial suppliers and used without further purification. THF was distilled from sodium/benzophenone. CH_3CN and CH_2Cl_2 were distilled from CaH_2. $MgSO_4$ was used as the drying reagent after aqueous workup. ^1H and ^{13}C NMR spectra were recorded on a Bruker AVII 500 at 500 MHz (^1H NMR) and 126 MHz (^{13}C NMR). NMR spectra were referenced to the residual solvent signal (^1H CD_2Cl_2: 5.32 ppm; ^{13}C CD_2Cl_2: 53.8 ppm) and recorded at ambient probe temperature. For simplicity, the coupling constants of the aryl protons for *para*-substituted aryl groups have been reported as pseudo first-order (i.e., doublets), even though they are second-order (AA'XX') spin systems. UV-vis measurements were carried out on a Varian Cary 5000 UV-Vis-NIR spectrophotometer at rt. Mass spectra were obtained from a Bruker maxis 4G. IR spectra were recorded on a Varian 660-IR spectrometer as solids in ATR-mode. Differential scanning calorimetry (DSC) measurements were made on a Mettler Toledo TGA/STDA 851e/1100/SF. Melting points were measured with an Electrothermal 9100 instrument. TLC analyses were carried out on TLC plates from Macherey-Nagel (ALUGRAM® SIL G/UV254) and visualized via UV-light (264/364 nm) or standard coloring reagents. Column chromatography was performed using Silica Gel 60M (Merck).

Triynes **1a** and **1b**,[i] and macrocycle **M1**[ii] were synthesized according to literature protocols.[iii]

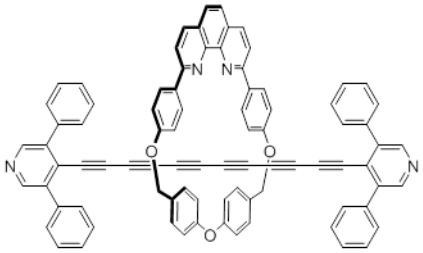

3•M1 from triyne 1a. TBAF (1.0 M in THF, 0.12 mL, 0.12 mmol) was added dropwise to a solution of **1a** (50 mg, 0.11 mmol) in wet THF (10 mL, and 0.05 mL of H_2O). The mixture was stirred at rt for 10 min, quenched via the addition of satd aq NH_4Cl (10 mL), and extracted with CH_2Cl_2 (2 × 10 mL). The combined organic phases were washed with H_2O (10 mL) and satd aq NaCl (10 mL). The solvent was reduced in vacuo to ca. 5 mL, and the mixture filtered through a plug of Al_2O_3 (EtOAc ca. 150 mL). The solution was concentrated under reduced pressure to ca. 3 mL. THF (5 mL) was added and the solution was concentrated to three mL. This procedure was repeated three times to displace as much of the EtOAc as possible, ultimately giving a solution of terminal triyne in THF (8 mL), which was used without further purification. In a separate flask, CuI (9.5 mg, 0.050 mmol) in CH_3CN (2 mL) was added to a solution of macrocycle **M1** (28 mg, 0.050 mmol) in CH_2Cl_2 (2 mL) and the mixture was stirred at rt for 1 h. The solvent was removed in vacuo and the residue dissolved in THF (3 mL). The terminal triyne in THF, as prepared above, K_2CO_3 (27 mg, 0.20 mmol), and I_2 (13 mg, 0.050 mmol) were added to the solution of the Cu-macrocycle complex **M1•CuI**. The reaction mixture was stirred at 60 °C for 24 h, cooled to rt, and quenched via the addition of CH_2Cl_2 (1 mL), CH_3CN (1 mL), and KCN (20 mg in 1 mL H_2O). After stirring for 2 h, the organic phase was separated, the aqueous phase extracted with CH_2Cl_2 (2 × 10 mL), and the combined organic phases were washed with H_2O (10 mL) and satd aq NaCl (10 mL). The solvent was removed in vacuo and column chromatography (Al_2O_3, hexane/EtOAc 4:1) afforded **3•M1** (1 mg, 2%) as a yellow solid.

3•M1 from triyne 1b. CsF (34 mg, 0.22 mmol) was added to a solution of **1b** (85 mg, 0.20 mmol) in wet THF (10 mL, 0.25 mL H_2O). The mixture was stirred at rt for 30 min, quenched via the addition of satd aq NH_4Cl (10 mL), and extracted with CH_2Cl_2 (2 × 25 mL). The combined organic phases were washed with H_2O (10 mL) and satd aq NaCl (10 mL), and dried ($MgSO_4$). The solution was concentrated under reduced pressure to ca. 5 mL. THF (10 mL) was added and the solution was concentrated to 5 mL. This procedure was repeated three times to displace as much CH_2Cl_2 as possible, ultimately giving a solution of terminal triyne in THF (10 mL). In a separate flask, CuI (14 mg, 0.072 mmol) in CH_3CN (3 mL) was added to a solution of macrocycle **M1** (40 mg, 0.072 mmol) in CH_2Cl_2 (3 mL) and the mixture was stirred at rt for 1 h. The solvent was removed in vacuo and the

residue dissolved in THF (6 mL). The terminal triyne in THF, as prepared above, K_2CO_3 (40 mg, 0.29 mmol), and I_2 (22 mg, 0.086 mmol) were added to the solution of the Cu-macrocycle complex, **M1·CuI**. The reaction mixture was stirred at 60 °C for 25 h, cooled to rt, and quenched via addition of CH_2Cl_2 (1 mL), CH_3CN (1 mL), and KCN (50 mg in 1 mL H_2O). After stirring overnight, the organic phase was separated, the aqueous phase extracted with CH_2Cl_2 (2 × 20 mL), and the combined organic phases were washed with H_2O (10 mL) and satd aq NaCl (10 mL). The solvent was removed in vacuo and column chromatography (silica gel, hexane/EtOAc 10:1, gradient to 1:1) afforded **3•M1** (11 mg, 13%) as a yellow solid. Mp 120–122 °C (decomp). R_f = 0.33 (hexanes/EtOAc 1:1). UV-vis (CH_2Cl_2) λ_{max} (ε) 478 (6250), 478 (6250), 434 (14000), 438 (12200), 404 (15600), 367 (65500), 351 (83900), 332 (78100), 316 (71600), 302 (59800), 281 (68300), 272 (70900), 259 (65100) nm; UV-vis ($CHCl_3$) λ_{max} 478, 438, 404, 368, 351, 331, 316, 272, 243 nm; UV-vis (toluene) λ_{max} 478, 439, 405, 368, 352, 333, 317, 284 nm; UV-vis (THF) λ_{max} 477, 437, 404, 365, 350, 331, 316, 271 nm; UV-vis (EtOAc) λ_{max} 475, 436, 402, 364, 348, 331, 315, 271 nm; IR (ATR) 3039 (w), 2928 (w), 2158 (w), 2048 (w), 1592 (m), 1489 (m), 1219 (s), 1180 (m) cm^{-1}. ^1H NMR (500 MHz, CD_2Cl_2) δ 8.58 (s, 4H), 8.27 (d, *J* = 8.3 Hz, 2H), 7.89 (d, *J* = 8.3 Hz, 2H), 7.79 (s, 2H), 7.75 (d, *J* = 8.7 Hz, 4H), 7.54–7.53 (m, 8H), 7.44–7.38 (m, 12H), 7.05 (d, *J* = 8.6 Hz, 4H), 7.00 (d, *J* = 8.6 Hz, 4H), 6.77 (d, *J* = 8.7 Hz, 4H), 5.20 (s, 4H). ^{13}C NMR (126 MHz, CD_2Cl_2) δ 159.4, 158.3, 158.1, 149.2, 146.8, 140.6, 136.8, 136.5, 134.3, 134.2, 129.9, 129.6, 129.0, 128.9, 127.7, 127.4, 126.0, 125.2, 122.1, 120.8, 116.2, 83.2, 73.7, 70.2, 70.1, 66.5, 64.3, 61.8. APPI HRMS (MeCN/toluene) calcd for $C_{84}H_{50}N_4O_3$ (M^+) 1162.3877, found 1162.3873; calcd for $C_{84}H_{51}N_4O_3$ ($[M + H]^+$) 1163.3956, found 1163.3944. DSC: Mp = 124 °C; decomposition, 142 °C (onset), 186 °C (peak).

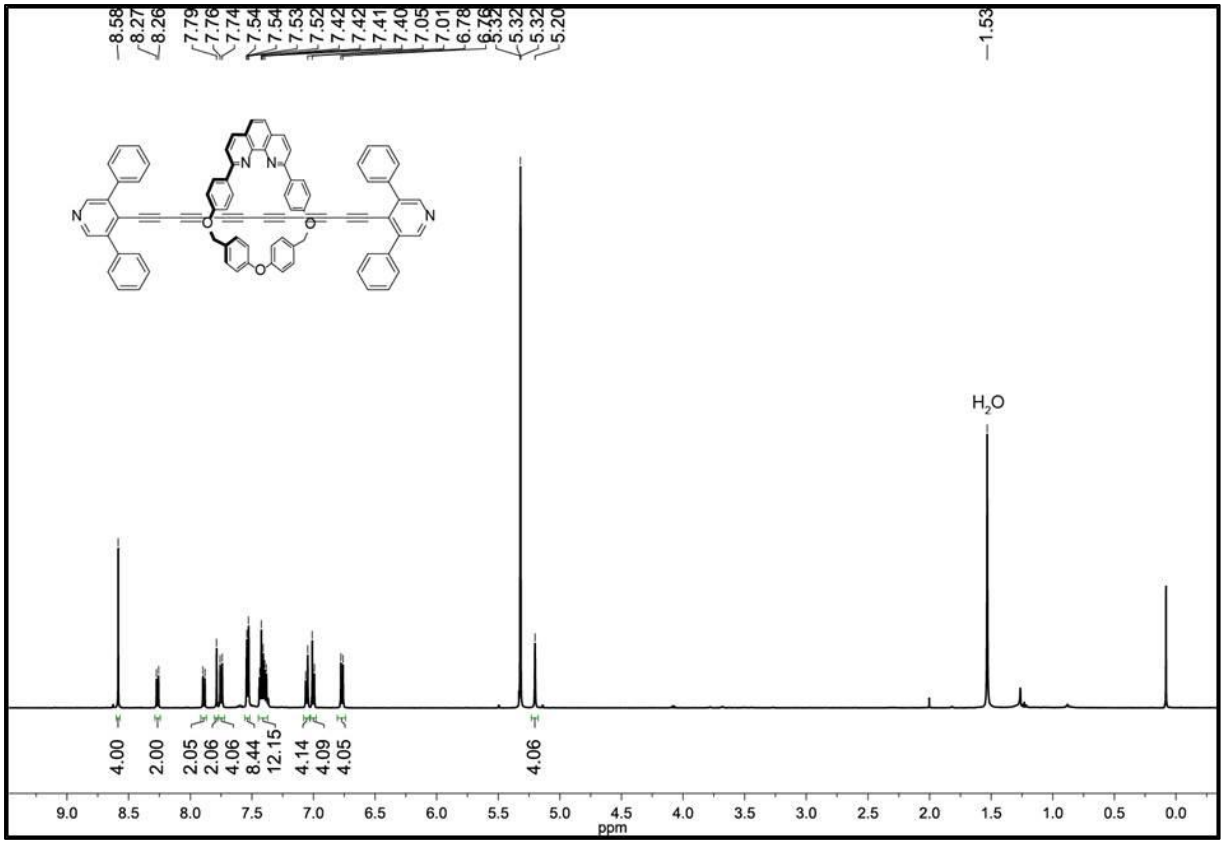

Figure S6. ^{1}H NMR spectrum of **3•M1** in CD_2Cl_2 (500 MHz).

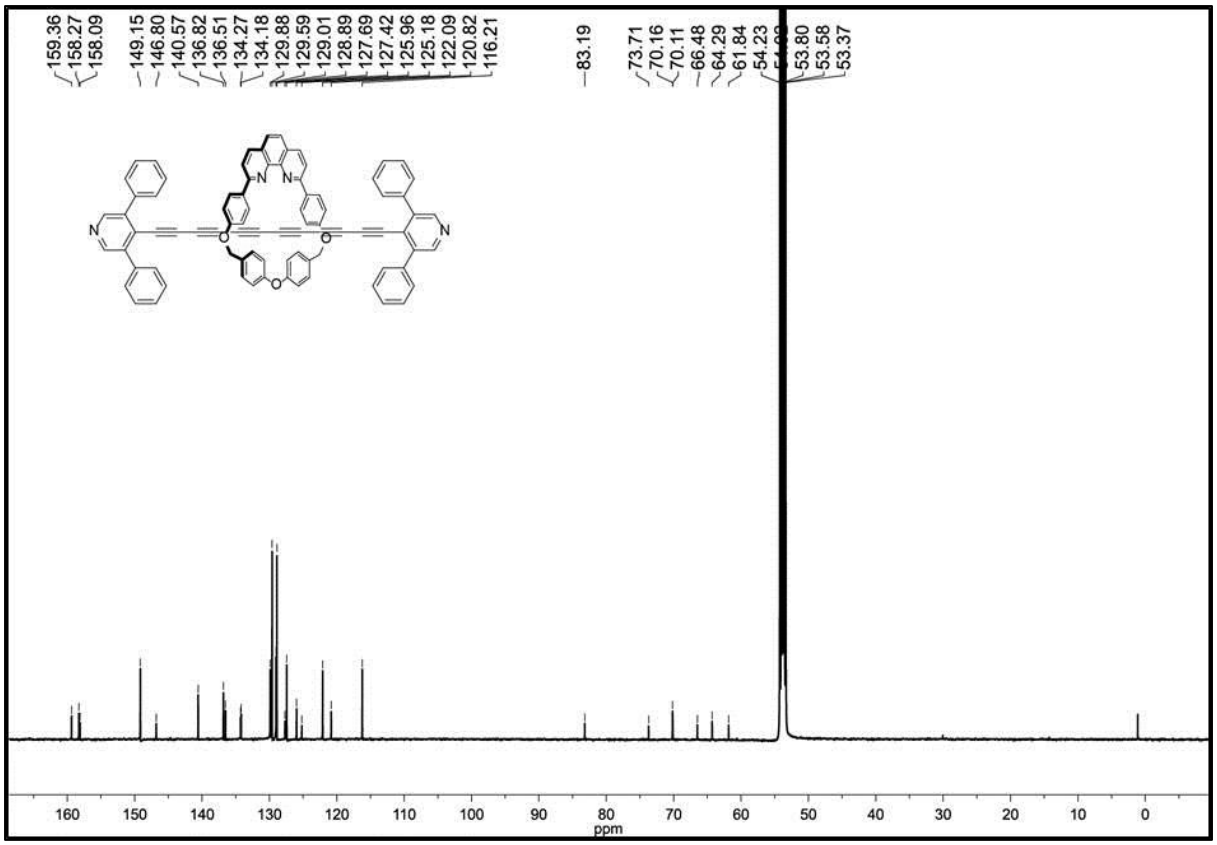

Figure S7. ^{13}C NMR spectrum of **3•M1** in CD_2Cl_2 (126 MHz).

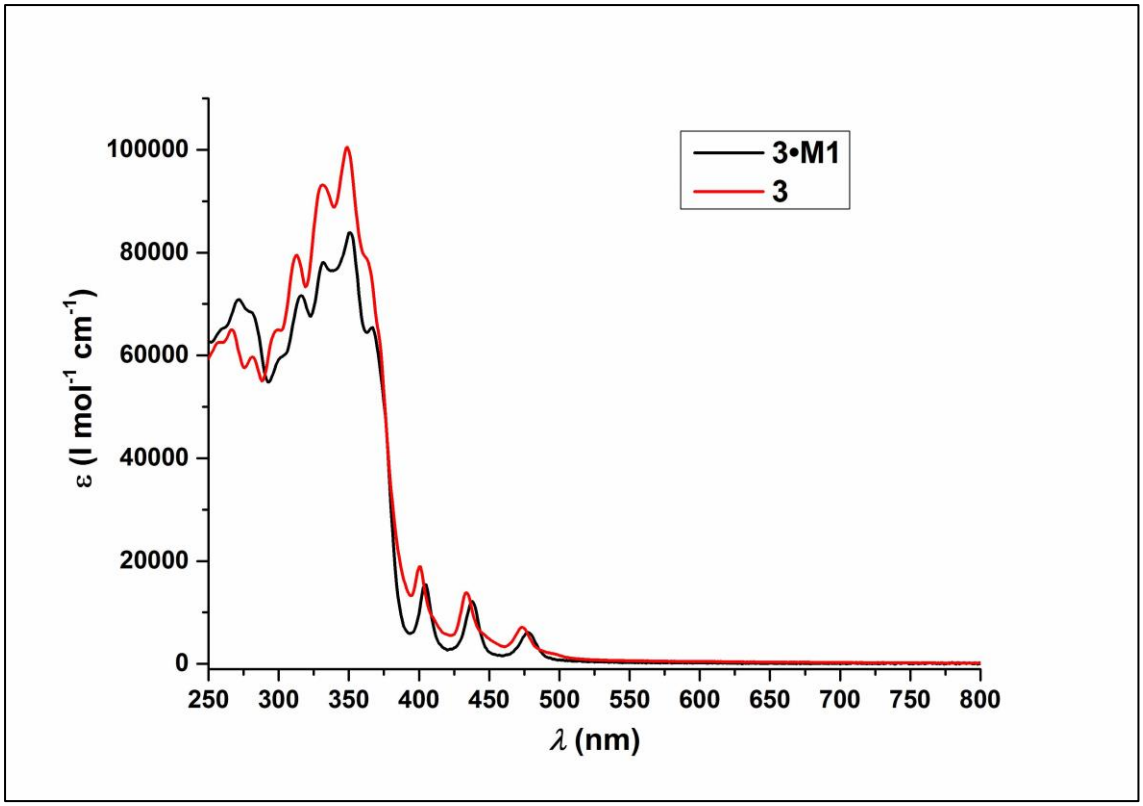

Figure S8. Quantitative UV-vis spectra of Dumbbell **3** and Rotaxane **3•M1** in CH_2Cl_2.

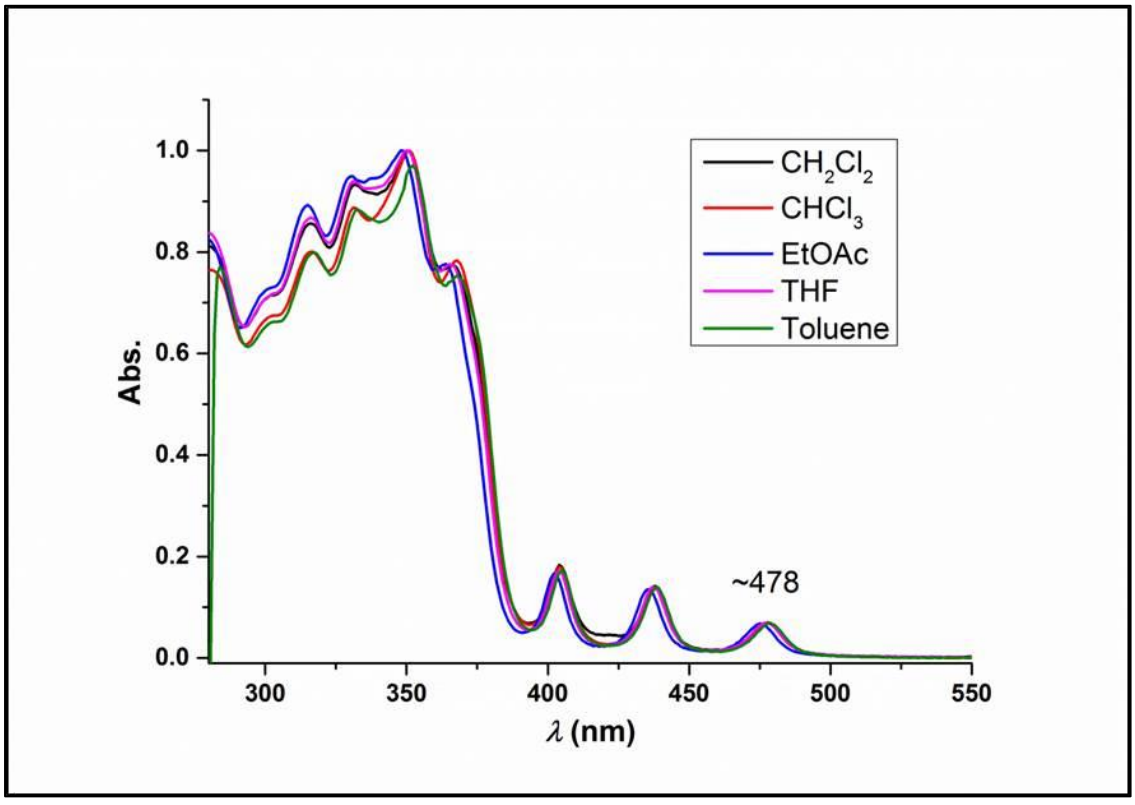

Figure S9. Solvent dependent UV-vis absorption spectra of Rotaxane **3•M1**.

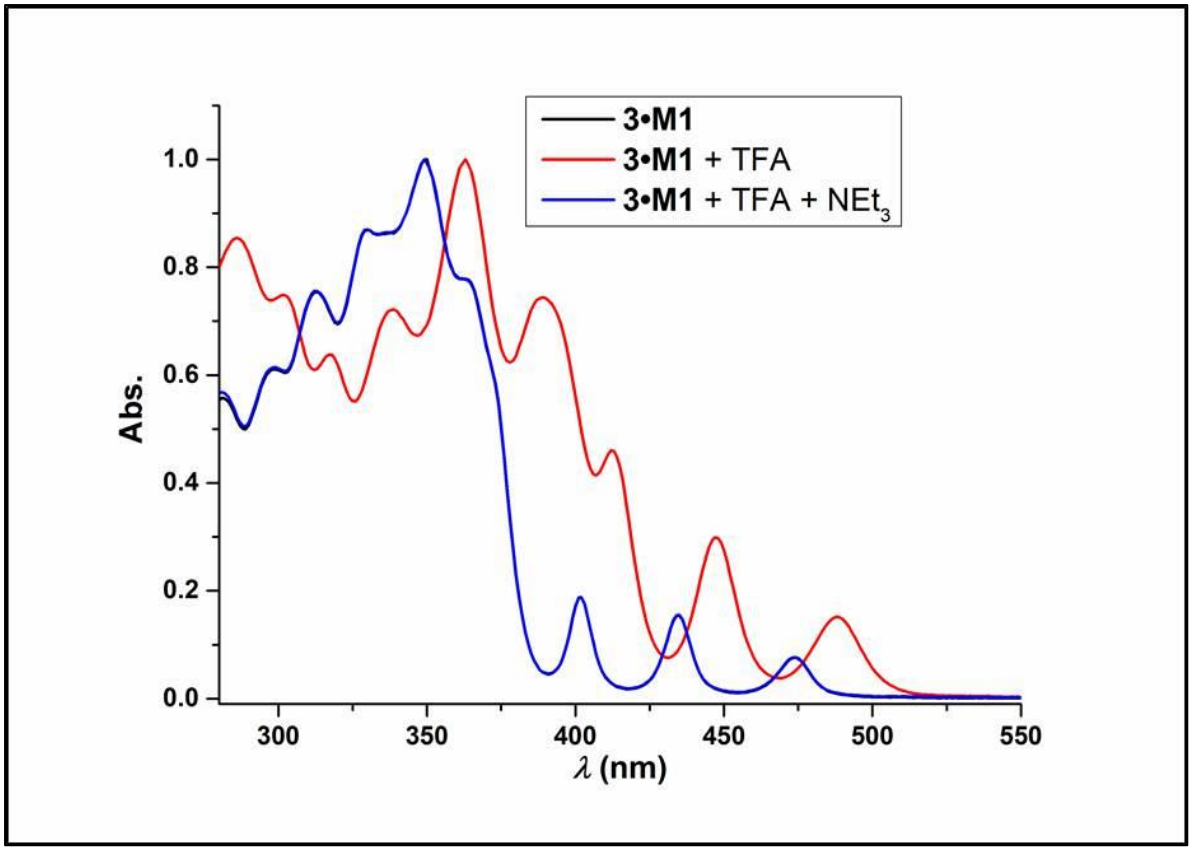

Figure S10. UV-vis absorption changes upon fully reversible protonation of rotaxane **3•M1** in CH_2Cl_2.

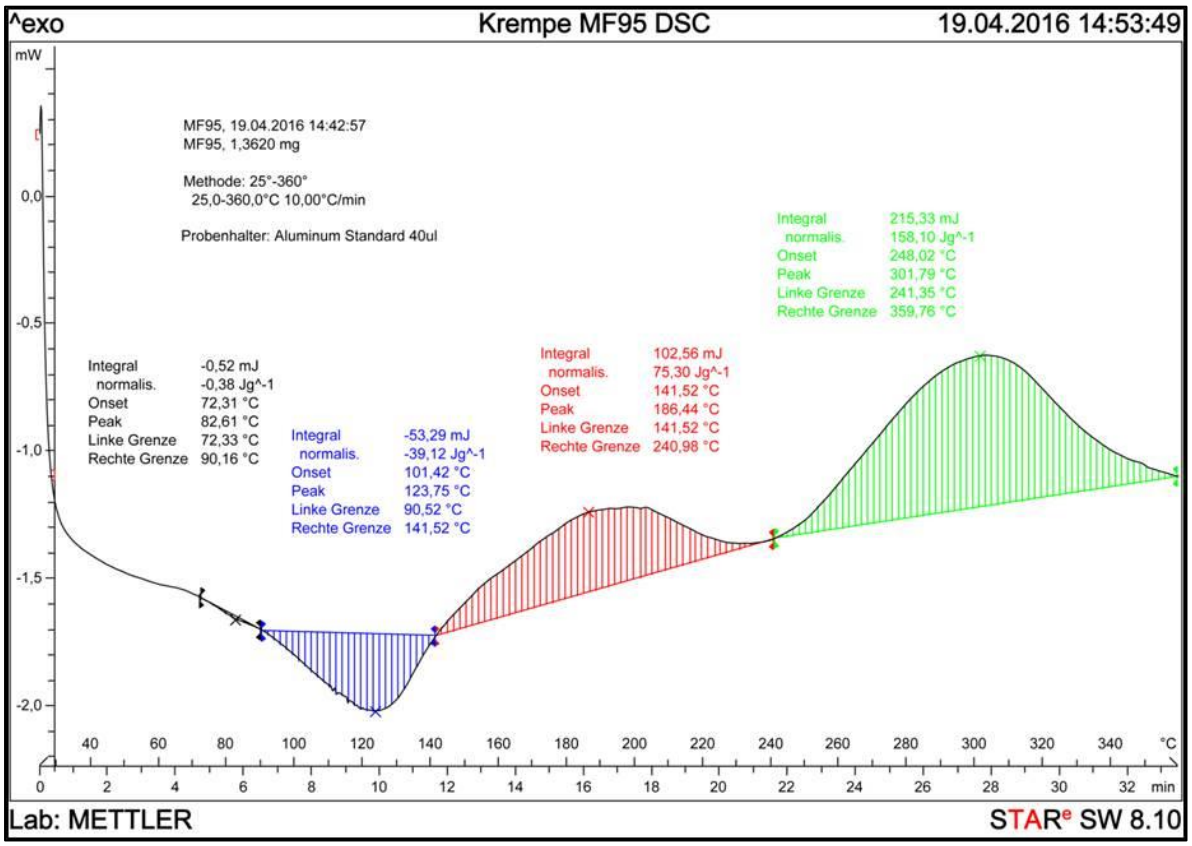

Figure S11. DSC trace of **3•M1**.

5. NMR spectra (1H and 13C) of the naked wire, macrocycle, and rotaxane.

Figure S12 shows ^{1}H NMR of the naked wire, macrocycle, and rotaxane and Figure S13 shows the corresponding ^{13}C spectra. These confirm that the spectra of the rotaxane are linear combinations of the individual components.

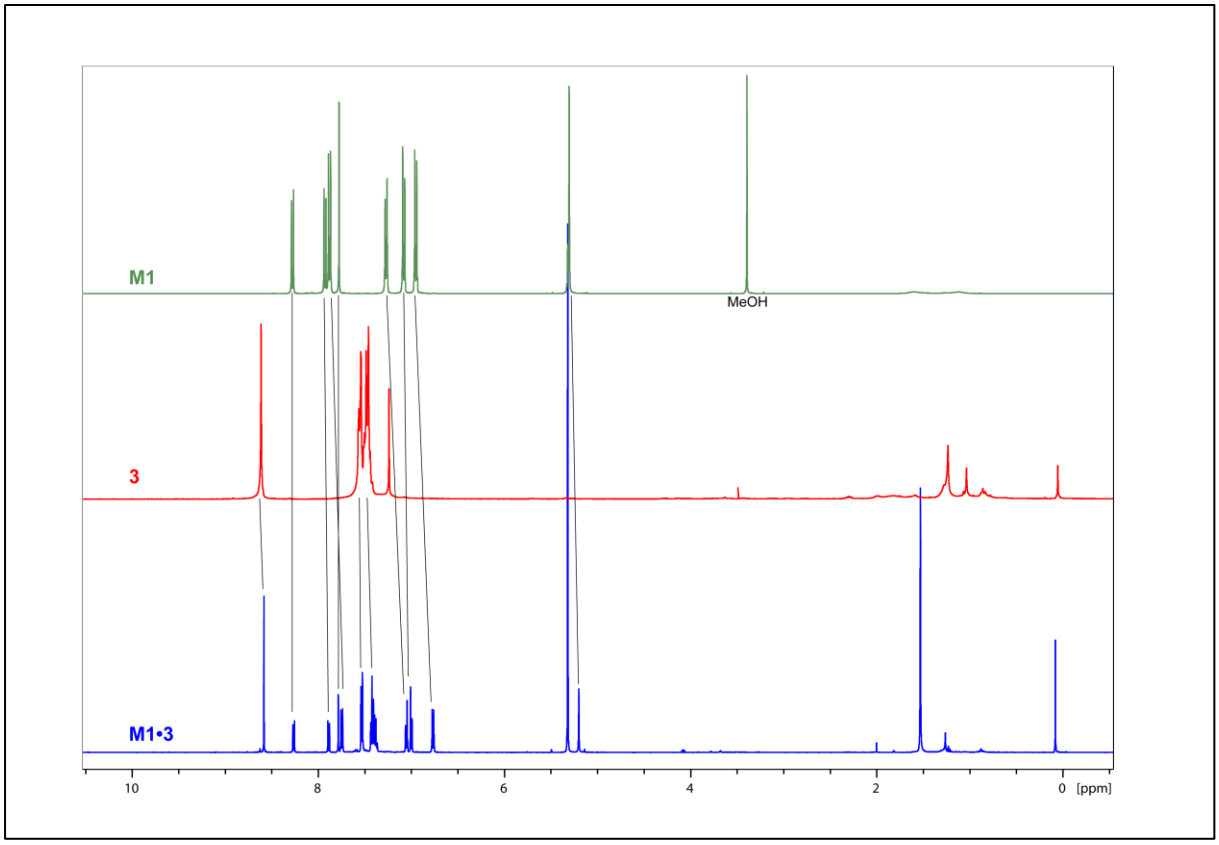

Figure S12. ^{1}H NMR spectral comparison of M1 (green, CD_2Cl_2), 3 (red, $CDCl_3$), and M1•3 (blue, CD_2Cl_2). Spectra of M1•3 are essentially a linear combination of the components M1 and 3.

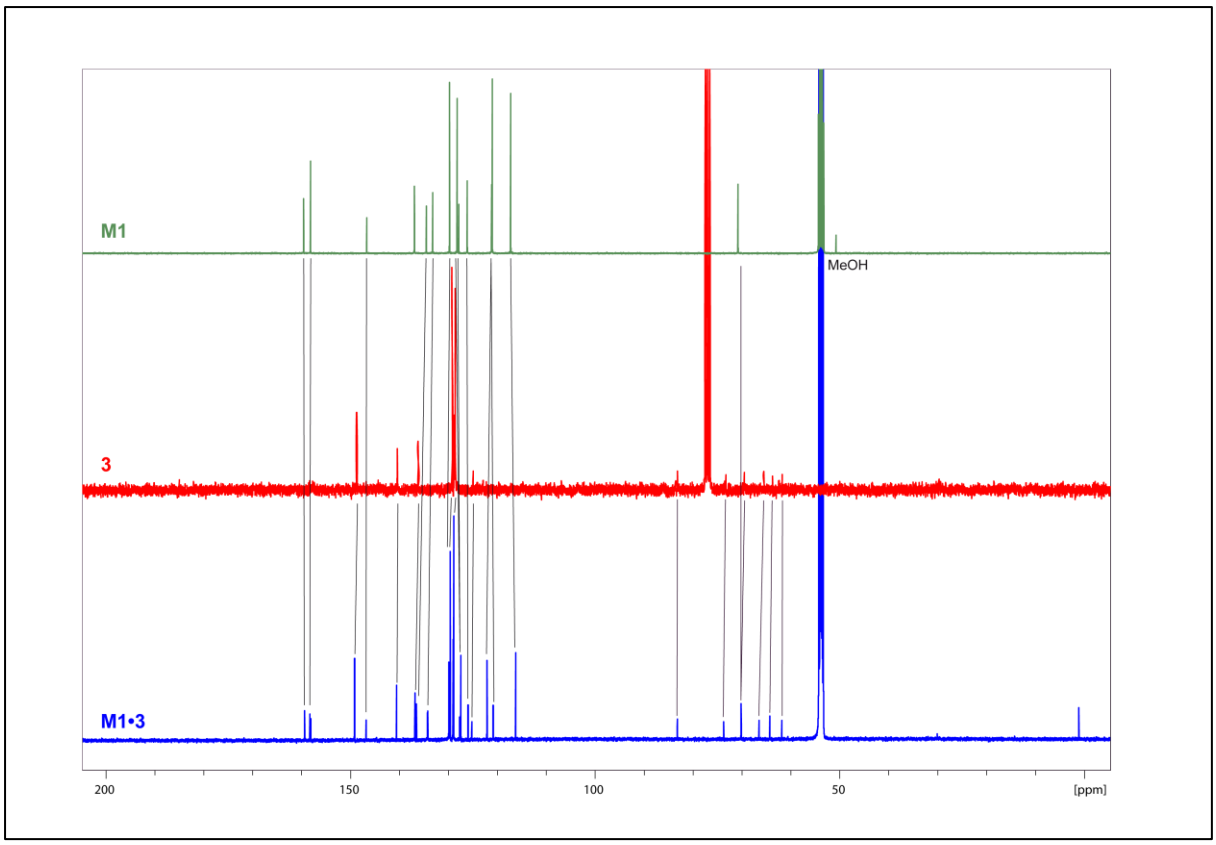

Figure S13. ^{13}C NMR spectral comparison of M1 (green, CD_2Cl_2), 3 (red, $CDCl_3$), and M1•3 (blue, CD_2Cl_2). Spectra of M1•3 are essentially a linear combination of the components M1 and 3.

[i] M. Krempe, R. Lippert, F. Hampel, I. Ivanović-Burmazović, N. Jux and R. R. Tykwinski, manuscript in preparation.

[ii] (a) A. M. Blanco-Rodríguez, M. Towrie, J.-P. Collin, S. Zališ and A. Vlček Jr., *Dalton Trans.*, 2009, 3941–3949. (b) M. Franz, J. A. Januszewski, D. Wendinger, C. Neiss, L. D. Movsisyan, F. Hampel, H. L. Anderson, A. Görling and R. R. Tykwinski, *Angew. Chem. Int. Ed.*, 2015, **54**, 6645. (c) L. D. Movsisyan, M. Franz, F. Hampel, A. L. Thompson, R. R. Tykwinski and H. L. Anderson, *J. Am. Chem. Soc.*, 2016, **138**, 1366-1376.

[iii] S. Saito,. K. Nakazono and E. Takahashi, *J. Org. Chem*., 2006, **71**, 7477–7480.